Properties Augmentation of Cast Hypereutectic Al–Si Alloy Through Friction Stir Processing

William P. Bates[1] · Vivek Patel[1] · Harikrishna Rana[2] · Joel Andersson[1] · Jeroen De Backer[1,3] · Mattias Igestrand[1] · Livan Fratini[2]

Abstract

The present endeavour is to augment mechanical attributes via friction stir processing (FSP) in hypereutectic aluminium–silicon castings by the means of microstructural modifications and defects reduction. Wherein, the study proceeds with mainly two approaches namely, alteration in tool revolution (TR) and the number of FSP passes. The prepared specimens were evaluated investigating volume fraction of porosities, microstructural characterizations and microhardness. Therefrom, the specimen with highest number of passes delivered most uniform properties resulting from the reduction in casting porosities and refined silicon particle uniform distribution throughout friction stir processed zone. This endeavour may be considered as a footstep towards more industrial readied material transformation.

Keywords Casting modification · Materials processing · Friction stir processing · Aluminium · Porosity · Grain refinement

Abbreviations

TR	Tool revolution
F	Feed
FSP	Friction stir processing
NP	Number of passes
SEM	Scanning electron microscope
OM	Optical microscopy
FSW	Friction stir welding
FSPed	Friction stir processed
PZ	Processed zone
TMAZ	Thermo-mechanically affected zone
HAZ	Heat affected zone
AS	Advancing side
RS	Retreating side
PM	Parent material
DRX	Dynamic recrystallization
T_{peak}	Peak temperature

Symbols

ω	Tool revolution
v	Feed
θ	Heat input efficiency
μ	Coefficient of friction
P	Pressure
R	Tool radius

✉ Vivek Patel
vivek.patel@hv.se

✉ Harikrishna Rana
harikrishnasinh.rana@unipa.it

1 Department of Engineering Science, University West, 46186 Trollhättan, Sweden

2 Department of Engineering, University of Palermo, Viale Delle SciePZe, 90128 Palermo, Italy

3 Friction Welding Process Section, TWI Ltd., Cambridge CB21 6AL, UK

1 Introduction

1.1 Casting Related Issues

Tracible back to approximately 3500–4000 BC, metal sand casting is one of the oldest known metalworking processes. The process is used not only for producing complex components but in a variety of shapes, sizes, and production volumes too catering to the industries such as shipbuilding, automotive, rail, defence, energy, and aerospace, etc. [1]. While the metal sand-casting process is an economical method for producing complex parts, it is prone to many defects, which affect the quality, integrity, reliability, safety, and acceptance of a final casting [2]. Common among these defects are gas porosity and shrinkage porosity [3, 4].

Porosity defects, such as these, are known to have an adverse effect on mechanical properties.

Simultaneously, Al–Si alloys have been attracting many industrial domains such as automotive, aerospace, etc. owing to their unmatched properties viz., high strength to weight ratio, exceptional wear resistance, and low coefficient of thermal expansion for a last few decades [5–7]. Especially the engine piston and engine block are the key applications from the sector which requires the combination of lightweight, toughness, and higher strength [6, 8, 9]. Still, with increased Si content coarse Si phase and other casting defects turn out to be inevitable through the casting route [7]. Consequently, those defects hamper the properties like impact toughness, strength, and ductility of the Al–Si alloy impeding its broader application. According to the data presented by Monroe, the ultimate tensile strength of an Al–Si alloy decreases approximately 125 MPa (11 KSI) in correlation to a 3% increase in hydrogen porosity [2]. Formerly, such casting process-related defects were mended employing arc welding. However, the latterly issues like oxidation, weak heat affected zone, deformation, and secondary cracks were reported owing to its procedural stages of high-temperature local melting followed by fast cooling [10–12]. More than a few other alternatives like alloying, rotary die equal channel angular pressing (RD-ECAP), heat treatment, and FSP have been used on Al-Si alloys to improve the impact toughness [6, 8, 9, 13, 14]. However, conventional methods such as alloy addition and heat treatments have been reportedly proven to be less advantageous compared to severe plastic deformation (SPD). On one hand, during SPD techniques no less than 8 passes of RD-ECAP were required to omit the voids left behind by the hard Si particles while on the other hand, only two FSP passes were reportedly enough to wipe out the greater part of the porosities from cast Al-Si alloy [15, 16]. This makes FSP a viable option to choose from.

1.2 Friction Stir Processing to Modify Cast Structure

In the last two decades, the FSP technology has evolved as an attractive alternative for surface and subsurface modifications. Solid-state, FSP technology was principally derived by Mishra et al. from the friction stir welding (FSW) technique [17]. FSP is principally a solid-state processing for modifying components using concentrated plastic deformation induced by a rotating tool. Producing low amounts of heat, FSP is effective at altering the surface/subsurface of aluminium alloys, with qualitative PZ, while negating many of the detrimental effects of fusion, such as porosity, cracking, and oxidation [18]. As reported by Rathee et al. the properties of the metal matrix not only depend on the reinforcement particles but also depend on the type, size, volume fraction, and spatial orientation of particles in addition to process parameters [7, 19, 20]. Proof of this can be found in FSP experiments performed by Sun et al.

who publicized the results exhibiting the reduction in pore morphology features, as well as intermetallic particle size for aluminium alloy A206 [21]. The grains were refined with a high ratio of high-angle grain boundaries to low-angle boundaries compared to what was observed in the as-cast alloy.

Simultaneously, in the Al–Si alloys employing multiple FSP passes has resulted in enhancement of grain refinement and further mechanical properties. As per all these reported investigations, maximum NP has downsized the primary aluminium grains alongwith secondary Si particles ensuing the mechanical attributes like yield and ultimate tensile strength, elongation, wear resistance, and tribological attributes along with corrosion resistance [16, 22–26]. For instance, Joshi et al. discussed the refinement of the detrimental second phase particles (Mg_2Si) resulting from FSP in AS21A magnesium alloy [27]. The microstructure was reportedly refined and almost freed from the porosity defects ensuing enhanced mechanical properties. At the same time, Yang et al. reported the breakage of coarse primary Si particles and acicular eutectic Si particles, elimination of porosity, and better homogeneity of Si particles attained from higher number FSP passes [28]. The impact toughness was enhanced by 7 times with the increase of the number of FSP passes (3) resulting from the reduction of Si particle average size and aspect ratio from 86.0 to 1.4 μm and from 3.42 to 1.48 respectively. Moreover, Prasad et al. documented about a 30% increase in YS and a 34% increase in UTS through three FSP passes with 100% overlap for as-cast Al–Zn–Mg–Cu alloy [29]. Although there is little research, to date, on repairing castings using FSP, experiments performed by Ruofei Huang et al., strongly suggest FSP is a viable alternative repair method to other aforementioned methods discussed [30]. Experiments herein are designed to evaluate the ability of FSP as a stand-alone process, to alter material properties or repair defects found on or near the surface of sand cast hyper eutectic Al-Si alloy plates, while avoiding some of the risks involved when weld repairing using a fusion welding process.

Therefore, it is desirable for the results of this experiment to produce outcomes where:

Volume fraction of porosity within the PZ shall be less than that of the "as-cast" PM.

Microhardness within the stir zone shall be greater than, or equal to, that of the "as-cast" PM.

Temperature throughout the friction stir process shall not exceed 660 degrees Celsius.

2 Materials and Methods

2.1 Friction Stir Processing

In total, nine experiments were made with an ESAB Rosio robotic system, using an FSP tool comprised a triflate pin

of 6 mm diameter and length 3 mm with a scroll shoulder of 12 mm diameter; shown in Fig. 1a. Al-Si alloy plate (EN AC-44100), 10 mm thick, 85 mm wide, and 135 mm long were subjected to FSP. The plate was fixtured in the robotic system separately and clamped using two-stepped strap clamps; shown in Fig. 1b.

The experiments were performed employing three variables viz., tool revolution- TR, tool feed- F, and the number of passes- NP varied in the range of 800–2000 rotation min^{-1}, 5–10 mm min^{-1}, and 1–5 respectively (see Table 1). The whole study was divided into two parts viz., "A" & "B". The objective of experiment set "A" was to study the influence of the number of FSP passes whereas set "B" was for different TR and F. The temperature at the FSP tool was measured using a Tool-Workpiece Thermo-couple (TWT) developed and configured by Ana Magal-haes, having one thermal couple wire connected to the top of the tool and another wire clamped beneath the corner of the plates [31]. Each FSP pass was carried out with an interval of at least 15 min to overcome the preheating and related defects. All data reported to the temperature control software, from the TWT, were recorded in 0.1-s increments from the start to finish of each FSP program for every pass encountered. The same is represented by a temperature plot depicted in Appendix A.

2.2 Microstructural Characterization

Microstructure specimens were sliced and eatched as pre standard metallurgical testing procedure (ASTM E 3–01, E407, E1920). All the samples aere etched using kellers etchant. Thereafter, several magnified images were captured of all samples using an Olympus BX60M light optical microscope. The best-processed samples (with least porosities and uniformly/high Microhardness) were further characterized Electron Backscatter Diffraction (EBSD) to infer about the grain morphology.

Table 1 FSP Parameters set

Experiment No	Tool rotational speed (RPM)	Axial Force (N)	Tilt (°)	FSP pass	Travel speed (mm s^{-1})
1	1500	4000	2	2	10
2	1500			3	10
3	1500			4	10
4	1500			1	10
5	1500			5	10
6	1000			1	10
7	2000			1	10
8	800			1	10
9	800			1	5

2.3 Microhardness and Porosity Measurement

Following preparations described in Sect. 2.2, samples were examined using a Zeiss AX10 light optical microscope. For FSPed specimens, 10×images were taken within the PZ area where the largest porosities could be positively identified. Whereas, for the PM sample, a stitched image at 10×magnification of the entire sample had been captured to optimize the amount of area, because of the larger size and nonuniform distribution of porosity. Microscope images were then used to measure porosity volume fraction, in the percentage of area, as well as size employing Zeiss software.

Vickers hardness testing had been performed on each sample. Using a Stuers Duramin 40 microhardness tester, tests were executed in a square pattern with a constant load of 200 g-force and a dwell time of 10 s. For processed samples, a square pattern comprised of 36 test locations had been placed symmetrically with respect to the centre-line of the PZ, approximately 1.5 to 2 mm beneath the top as depicted in Fig. 2. Whereas, the parent metal sample, labelled "PM", had been tested in a centroid square pattern comprised of 60 test locations spaced 1 mm apart. Immediately following each test, every indentation had first been

Fig. 1 Experimental set up: **a** FSP tool schematic **b** FSP-plate clamping layout

(a)

(b)
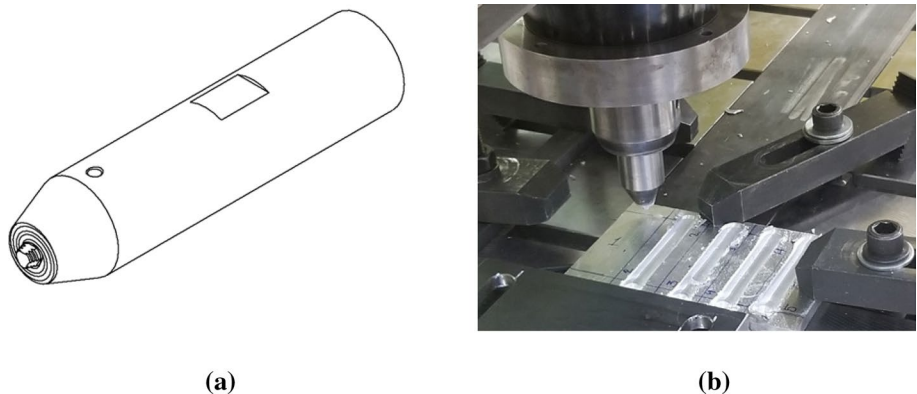
automatically measured then verified by the operator under 10× magnification.

3 Results & discussion

3.1 Temperature analysis

Temperatures have been measured at the point of contact of the FSP tool, and temperatures distribution curves for all FSP samples are plotted in Appendix A. Measurements taken during welding recorded peak welding temperatures ranging from 435 to 554° C with a standard deviation of 29° C (refer Fig. 3). Although the TWT exhibits accuracy

limitations during plunging after the tool submerge, temperatures stabilize, and for this report shall be considered to be accurate. Because temperatures of the inter-pass welds have identical FSP parameters, measurements and results thereof, are delineated using a suffix representing the inter-pass number. In an example, "P2" is affixed to the end of the root designation for the second FSP pass; wherefore, "R1500104P2" is the second pass of the four-passes, multi-pass weld.

The FSP program for specimens R0800101 through R2000101 which were processed with higher F (@ 10 mm s^{-1}) ran for approximately 21 to 27.6 s. Beginning with an initial contact temperature of approximately 25 to 32 °C, these passes reached their modal pass temperature 11.7 to

Fig. 2 Hardness indentation map in nugget zone
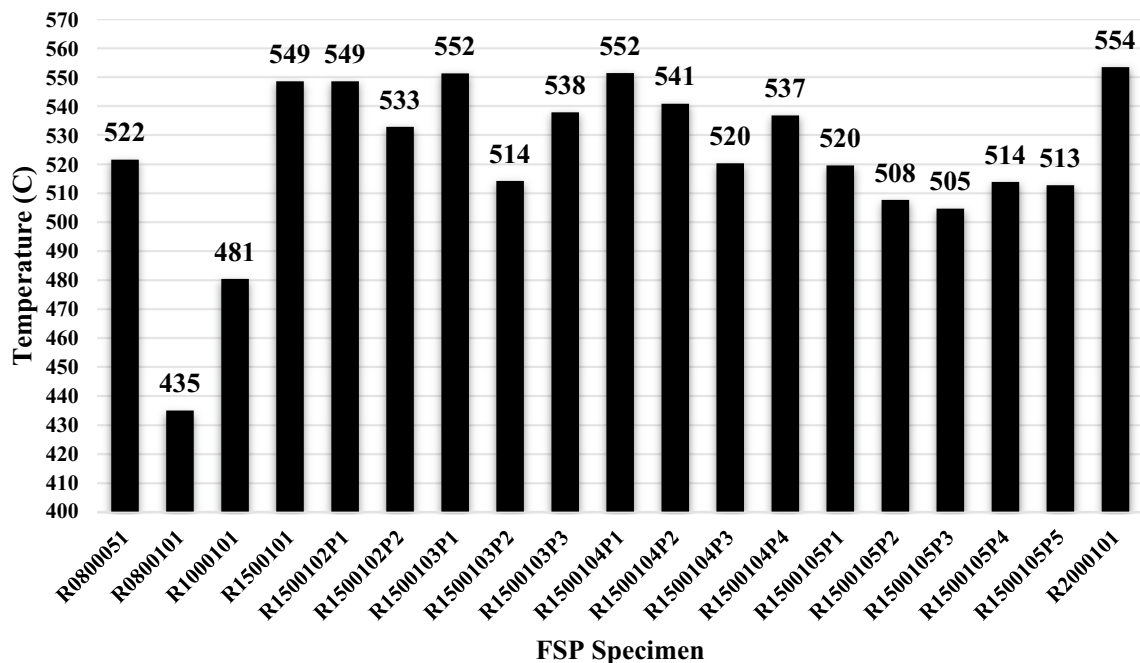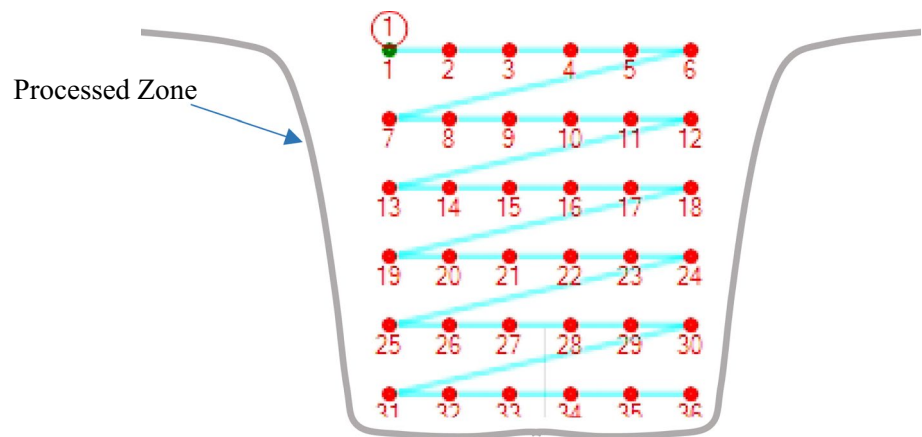
Fig. 3 Peak temperature plot

15 s into the program and 8.7 to 12 s after initial contact. Whereas program R0800051 which was processed with a low F (@ 5 mm s^{-1}) had a duration of 12.5 s, reached its modal pass temperature after 2 s into the program.

It was noticed while comparing the peak temperatures of the specimens R0800051 and R0800101 that the R0800051 specimen exhibited higher peak temperature as compared to others. The lessening of F, keeping TR constant upsurges the time of tool shoulder-substrate interaction, followed by higher friction and deformation of substrate ensuing into higher peak temperature [32, 33]. This elucidation can further be verified by the heat model recommended by Frigaard et al. through the following Eq. 1 [34].

$$H = \frac{4}{3}\pi^2 \frac{\infty P \mu \omega r^3}{v} \tag{1}$$

(Here, H = average heat input, Ø = heat input efficiency, µ = coefficient of friction, P = pressure (Pa), ω = tool rotation speed, r = tool radius (meter) and v = tool traverse speed) This model can be further simplified by the following equation:

$$H \propto \frac{\omega}{v} \tag{2}$$

In accordance with Eq. 2, the value of v is inversely linked to heat input which authenticates the rise of peak temperature with reduced v. Conversely, the increase in v cuts the residing time of the frictional heat resulting in lower peak temperature [33, 35]. Also, the increase in the value of ω which is directly proportional to heat input upsurges the peak temperature as recorded in the samples R0800101 through R2000101.

Moreover, an interesting pattern of the peak temperatures was noted in the number of passes study. The first pass for all the FSP programs (R01500101 through R1500105) exhibited the highest peak temperature among all owing to maximum resistance experienced by the tool to deform the immaculate PM and believed to be gradually dropping with subsequent passes. Metaphorically, in the first 3 passes of the 4-pass specimen, temperatures gradually decrease from 552 to 520 then rise to 537 in the 4th pass. However, there were some exceptions like the 5-pass specimen in which the temperature pattern of the 5-pass specimen is reasonably static, beginning with 508, peaking at 520, and finishing at 513. Regardless of processing parameters, each FSP pass appears to reach a certain temperature threshold limit and maintains that temperature threshold until the processing is terminated. This observation is consistent with the known "self-limiting effect" of friction-heated processes, or "fully coupled thermomechanical processes" [36].

## 3.2 Macro & Microstructure: Particle & Grain Refinement/Reorganisation

The cast Al–Si microstructure is primarily comprised of an α-aluminium matrix, as non-faceted dendrites, and silicon precipitates. Given the relationship between microhardness or yield stress and primary dendrite arm size/spacing can be estimated using the equation (Eq. 3):

$$\sigma_y = \sigma_0 + k\lambda^{-1/2} \tag{3}$$

which had been derived from the hall-patch equation [37]. Here, k is Hall–Petch slope, and λ is microstructure length scale such as average grain size or interlamellar spacing [38–40]. Reduction in sizes of both the aluminium dendrite arms and silicon lamellas reduces the spacing among the dendrites which ultimately increases the yield stress and microhardness. Additionally, the α-aluminium matrix is prone to dislocations which are typically reduced through the introduction of silicon precipitates. However, silicon tends to fail from brittle fracturing induced by stress concentration on silicon lamellas. The risk of brittle fracturing in Al-Si can also be mitigated by a reduction in the size of the silicon lamella, as well as transforming the silicon precipitates from lamella to spheroidal [41, 42]. The size and spacing of silicon lamella for raw Al-Si cast plate have been estimated using the measurements recorded in Fig. 4a, b. Large concentrations of α-aluminium separate fields of silicon precipitates and range in size approximately 36 µm to more than 500 µm; whereas, spacing of the silicon lamella, as indicated by λ in Eq. 3, within the fields of silicon range approximately 0.5 to 5 µm. The length of the silicon lamellas themselves measure approximately 1 to 13.3 µm in length, and 0.1 to 2.5 µm in width.

However, the FSP led enormous plastic deformation altered the microstructure with the substantial transformation of Si particles and precipitates along with grain refinement. Identical particle breakdown has also been reported by Sung et al., where they found small fragments of AA 3003 into AA 6013 during the course of multilayer FSW [43]. The particles are swirled and fractured by the combination of tool compression and shearing engendered through FSP tool [44]. Further evaluation of the microstructures within the PZ as displayed in Fig. 4c–k, show the silicon lamella have also been broken and uniformly redistributed throughout the α-aluminium matrix. The silicon lamella has been reduced in length and made more spherical in all-welded samples. To compare this transformation to the PM, measurements were collected of the approximate size range and maximum spacing of silicon precipitates and are listed in Table 2. From the observations and measurements, it can be said that the length of the silicon lamella has decreased at most 96% and the maximum spacing has reduced, at most, by a factor of 29.
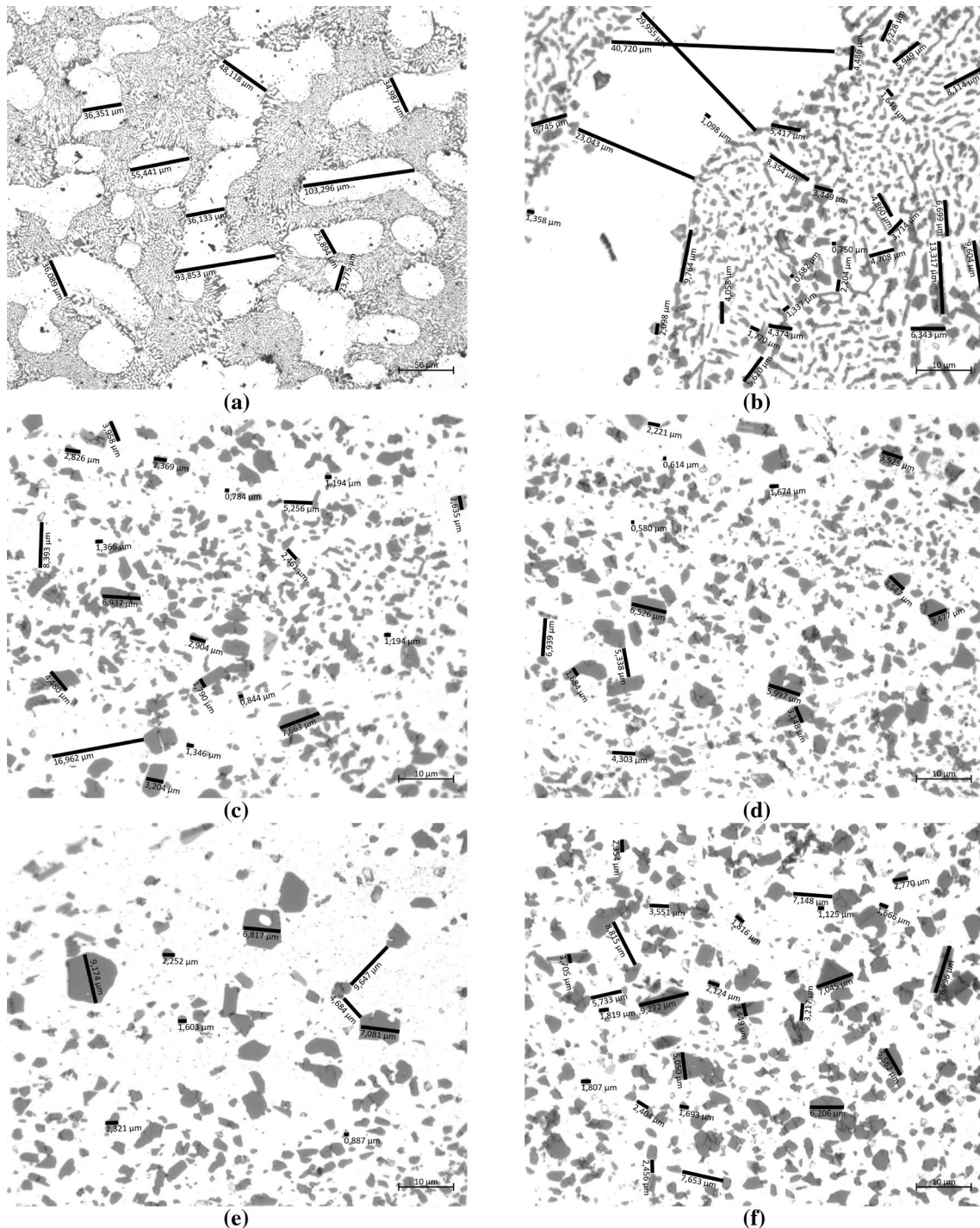
Fig. 4 Si Particle distribution resulted from FSP for samples: **a** PM×20 **b** PM×100 **c** R0800051×100 **d** R0800101×100 **e** R1000101×100 **f** R1500101×100 **g** R1500102×100 **h** R1500103×100 **i** R1500104×100 **j** R1500105×100 **k** R2000101×100

On the other hand, the grain morphologies have also been largely influenced by the TR and FSP multiple passes. As being a thermo-mechanical process FSP leads to grain refinement in consort with particle refinement. The measured average grain size for the unprocessed PM was 175 ± 10 μm which was downed to 4 ± 1.2 μm with the finest microstructure recorded for the highest TR of 2000 rotation min^{-1}, assuring the stronger thermomechanical mixing of the structure caused by the FSP. The EBSD analysis revealed through crystallographic triangle, [001] orientations for the majority of the Al-Si substrate matrix grains which was distorted to [101] and [111] orientation with refinement. The

(g)

(h)

(i)

(j)

(k)
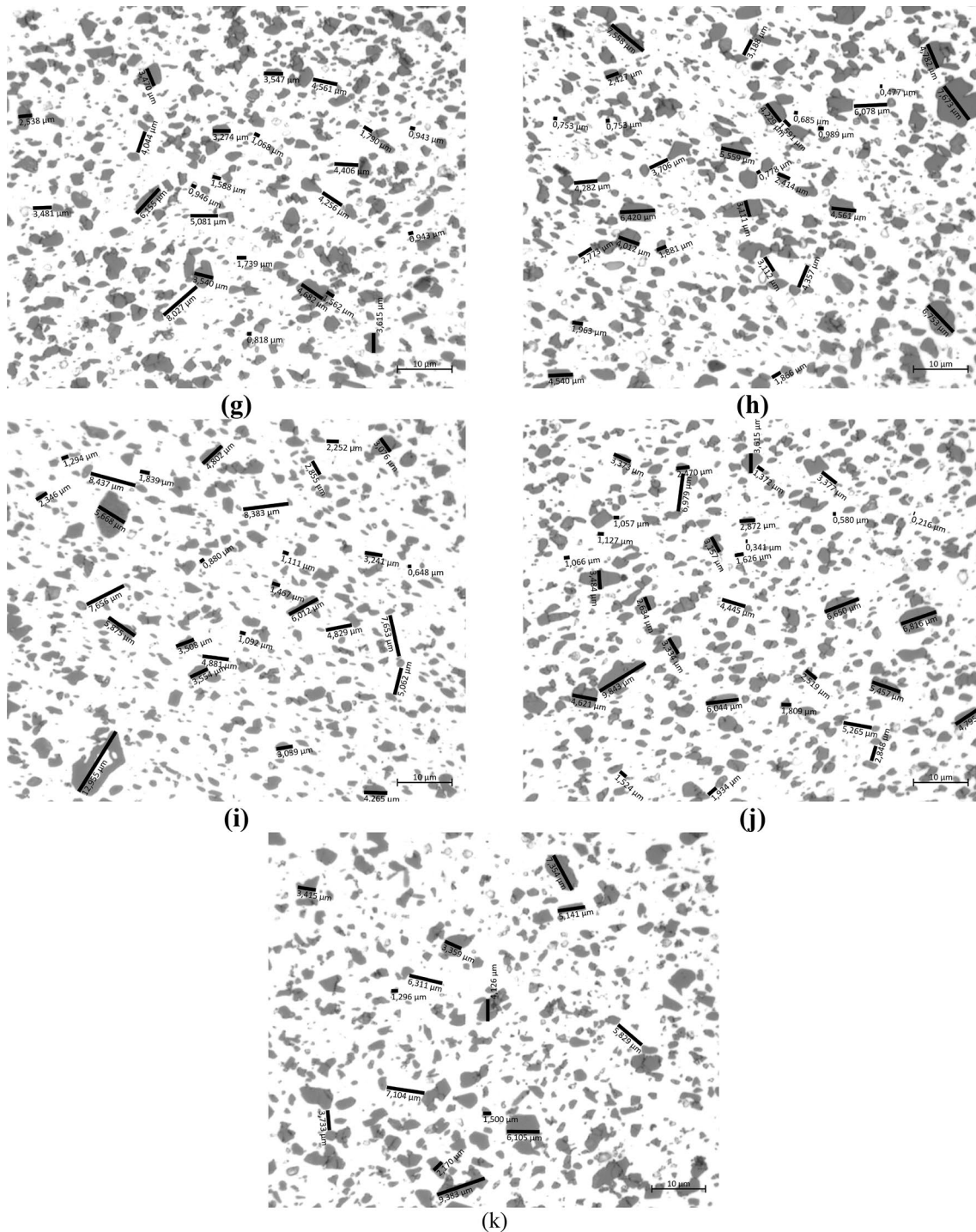
Fig. 4 (continued)

EBSD maps of the FSPed specimen with the highest TR of 2000 rotation min^{-1} are exhibited in Fig. 5a, which indicates fine-equiaxed grains. As it can be seen from Fig. 5b, the large fraction of the grain size was found under 8 μm. Along with the grain refinement, more than 81% of the grain boundaries were transformed to a high angle ($> 15°$),

as shown in Fig. 5c. The majority of the grain refining technologies require multiple steps or passes in order to realize substantial grain refinement [45]. The fine equiaxed grain morphology can be attributed to the temperature of deformation all through FSP. It is generally noticed that the deformation becomes more homogeneous as the temperature of

Table 2 Microstructure measurements

Sample	Length & width (μm)	Spacing (MAX)
R0800051	0.8 to 7	17
R0800101	0.5 to 7	7
R1000101	0.8 to 9.3	9.7
R1500101	1.6 to 9.3	9
R1500102	0.9 to 6.2	8.5
R1500103	0.5 to 7.7	6
R1500104	0.6 to 10.2	8
R1500105	0.5 to 9.9	5.3
R2000101	1.2 to 9.4	5.9

deformation increases [46]. Moreover, in the words of previous investigations dynamic recrystallization (DRX) has been considered as the principal grain refinement mechanism in the PZ of FSPed specimens [20, 47–51].

Nevertheless, as per as the influence of the number of passes is concerned after 1st pass the grain refinement did not exhibit a significant reduction. At the same instance, there was not any established relationship between the number of passes and grain sizes. Emblematically, for the initial one to two passes the grains were refined marginally high as compared to subsequent passes yet with a further number of FSP passes grain sizes were increased in several instances owing to distinct FSP thermal cycles. Such outcomes signpost that the final grain size in the PZ does not rely on the
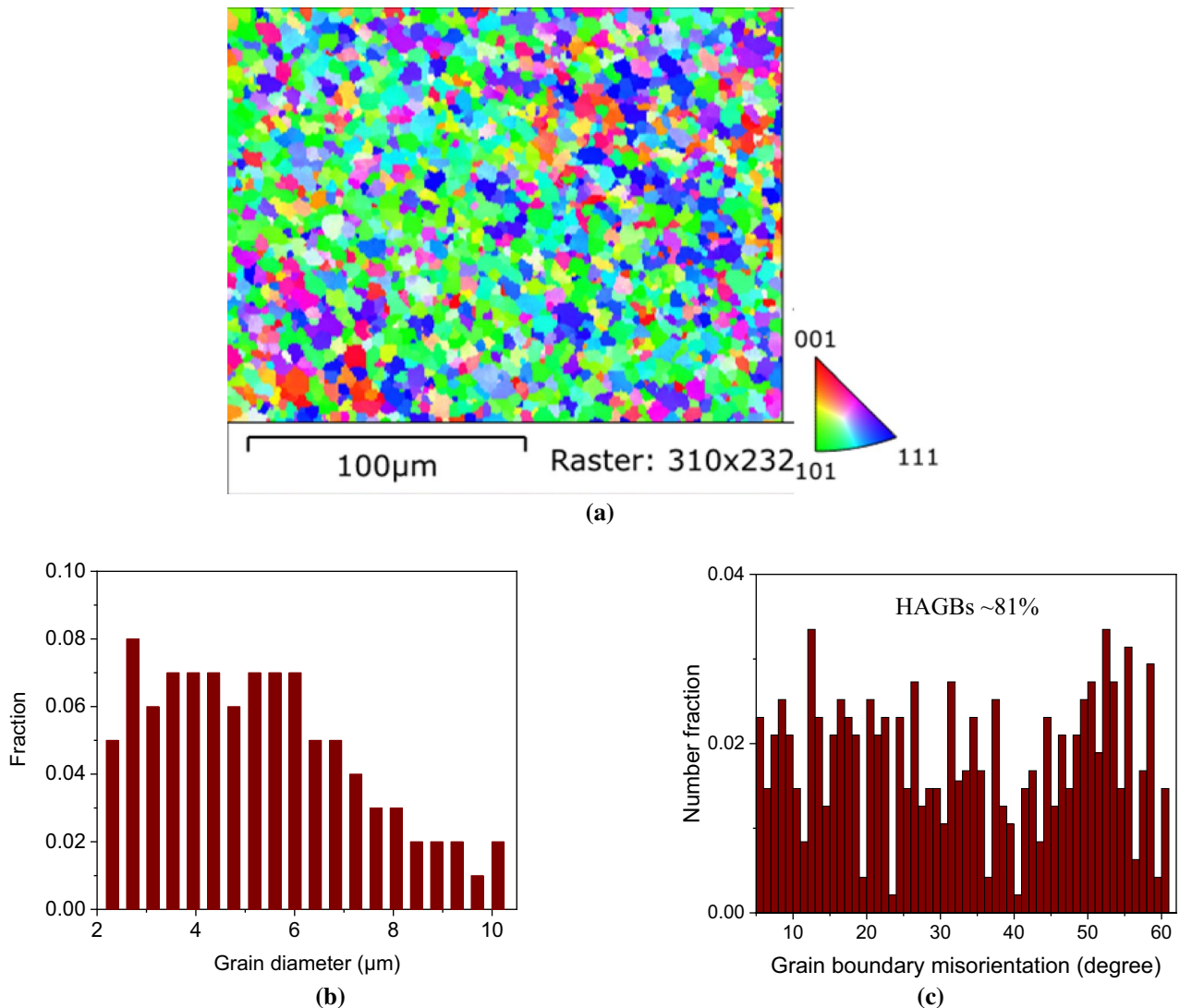
Fig. 5 EBSD analysis of sample R2000101(@2000 rotation min^{-1}; 10 mm min^{-1}): **a** grain orientation map, **b** grain size distribution, **c** grain boundary misorientation distribution

preliminary grain size but the process parameters. Alike outcomes have been publicized for the case of multiple pass FSP of pure aluminium [52, 53]. A large amount of plastic strain in the aluminium PM generated by the extreme plastic deformation during the course of FSP heightens the dislocation density. The elevated temperatures caused by this intense plastic deformation and friction through shoulder-substrate interaction result in recovery and recrystallization [54]. Whereas recovery dominates at elevated temperatures owing to its low energy ingesting attribute, FSP led heightened dislocation density promotes the dynamically recrystallized grains. Hence, with multiple passes recovery may be dominant leading to the larger grains in the PZ.

Besides, the shattered micro-sized Si particles present in the PM can act as apposite nucleation sites for the novel grains [33, 55–57]. These particles further augment the DRX mechanism by the particle-stimulated nucleation (PSN) mechanism. However, as reported by Ardakani and Humphreys the critical particle size required for the PSN mechanism is about 1 μm [58]. Accordingly, the existence of submicron-sized Al-Si particles in the PZ acted as nucleation sites for new grains resulting in grain refinement through the PSN mechanism.

3.3 Porosity

It is an undeniable fact that FSP engenders the viscoelastic material flow through thermomechanical processing, not only aids in refining the microstructures but the defect reduction too. It is clearly evident through the macrostructures depicted in Fig. 6 that during FSP the increase in the NP has played a pivotal role in reducing the number of defects like porosity, cracks, etc. To evaluate further the role of all the parameters the porosity map for distinct FSPed specimens and PM has been exhibited in Fig. 7. To observe the relationship between porosity volume fraction and each processing parameter, % volume fraction measurements, collected in accordance with Sect. 3.3, have been compiled in, Fig. 8. Wherein, "0" represents the PM sample. It should be noted that, due to the distribution of porosity within the PM, the data collected from the surface area of sectioned samples is not enough to represent the entire body. However, the general behavior of the FSPed region can be derived from Fig. 8a–c. Thereby, comparing all it can be said there is a significant size reduction, and redistribution of porosities.

Taking into consideration the porosity volume fraction measurements with respect to processing parameters, Fig. 8b suggests that there is just about a linear relationship between TR and porosity volume fraction. Given that porosity percentage has been declined by 40 to 70% for the TR of 800 to 2000 rotation min^{-1}. Finally, Fig. 8c indicates porosity reduction results for 800 rotation min^{-1}, in which reducing the feed F from 10 to 5 mm s^{-1} downs the porosity fraction

owing to the comparatively higher FSP processing time and thereby plastic deformation. Further examination of the entire PZ, in each sample, suggests the reduction in porosity could be the result of displacing material from other areas of the PM. Moreover, the displacement depth has reportedly increased with the NP as indicated in Table 3. Simultaneously, the volume fraction of the porosity is reduced with the increase in the NP with the almost linear relationship as the amount of visco-plastic material flow surges with each additional FSP passes and ensuing the redistribution of material within PZ. Interestingly enough, the single-pass weld at 2000 RPM has the lowest area percentage measurement for porosity, no cavity defects, and a displacement depth of 129 μm. In each FSP pass, closure of porosities and rearrangement of the Si particles occurs due to the intensified stirring effect [23].

3.4 Microhardness

Vickers microhardness test measurements have been performed in accordance with Sect. 3.3. To this end, microhardness averages are compared for FSP parameters: TR, NP, and F (Refer Fig. 9). Additionally, having calculated standard deviation from each test result for each sample, it considered to represent the uniformity of microhardness throughout an individual sample; shown in Fig. 10, because microhardness tests were evenly distributed over a given area.

Apparently, a positive trend was evident in the graph establishing the relation between the microhardness and TR. From the graph depiction almost a 17% rise in the microhardness was recorded with the specimen FSPed at maximum TR of 2000 rotation min^{-1}. Thereby, the average HV 0.2 microhardness measurements increased from 6% for 800 rotation min^{-1} to 17% for 2000 rotation min^{-1}. Such an upsurge can be attributable to the uniform distribution of Si particles in the aluminium matrix, porosity reduction, accompanied by the grain alteration encountered by DRX and PSN mechanisms as conferred in Sects. 3.2 and 3.3. Moreover, Rana et al. revealed the way in which these fine Si particles and fine grains bid higher microhardness through discrete strengthening mechanisms [33].

Firstly, in service the load applied to the aluminium matrix is shifted to Si particles dispersed in the PZ through confluence shear stress as per the shear lag mechanism [59]. The dislocation movement and further plastic distortion are restrained by this shear stress. Secondly, there is an undeniable role of the work hardening mechanism in the strengthening of the substrate. The geometrically indispensable dislocations adjacent to Si particles are engendered owing to a large disproportion amid coefficient of thermal expansion of aluminium matrix and the Si reinforcement particles all through the cooling period after thermoplastic deformation [60]. These dislocations further restraint the plastic

1 Pass | 2 Pass

3 Pass | 4 Pass

5 Pass
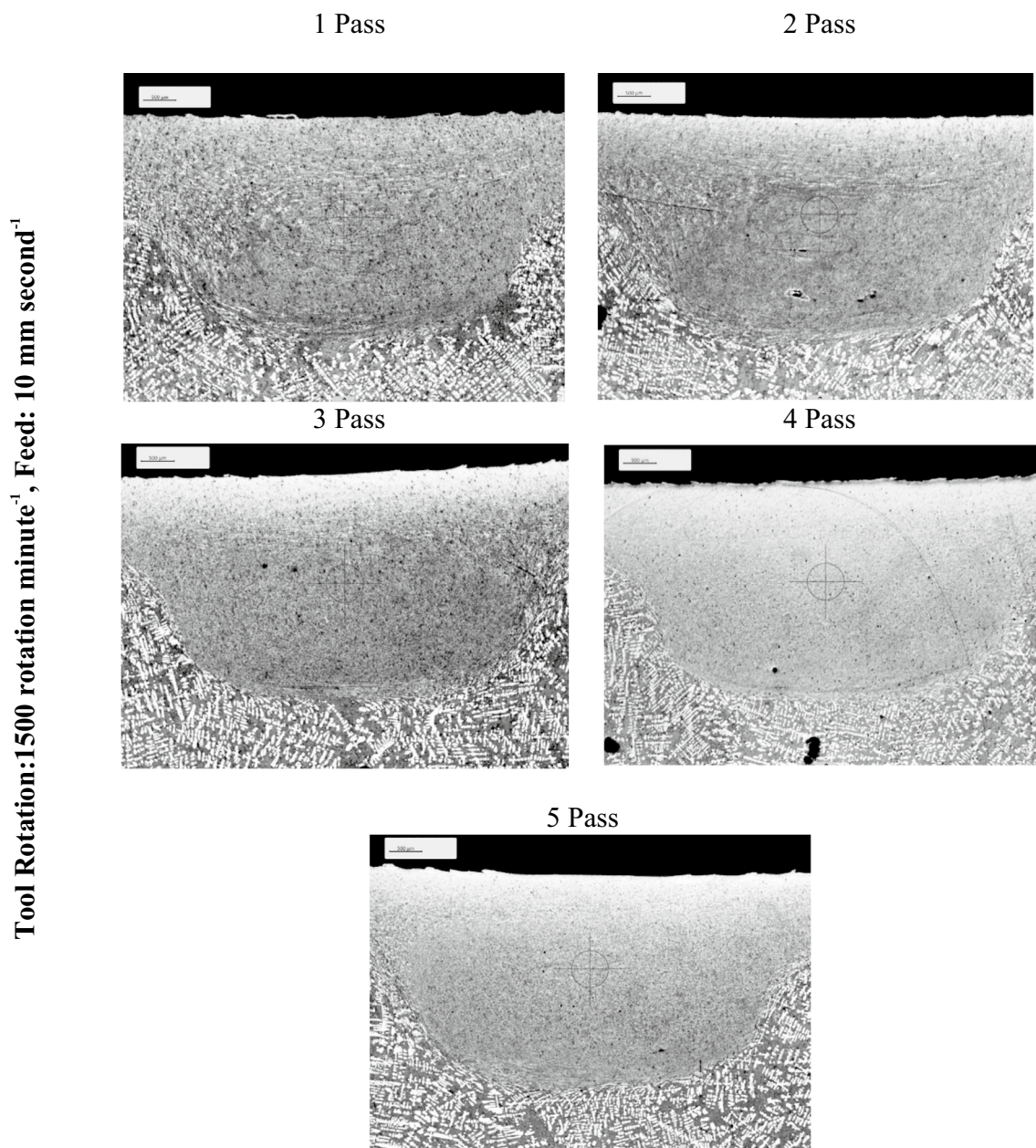
Fig. 6 Macrostructures of the specimens FSPed with different number of passes

deformation and enhance yield strength and microhardness as well as ensuing work hardening of the PZ. Apart from these mechanisms, with higher grain boundary area envisaged through FSP led refined grains further interrupts the dislocation movement and thereby enhances the microhardness [61]. Like other parameters, FSP at 5 mm s^{-1} shows an increase of microhardness from the PM, which appears to have a relationship with the amount of "stirring". However, a minuscule rise in the microhardness was registered by reducing the feed by 50% from 10 to 5 mm s^{-1}.

On the other hand, comparing the average microhardness of multi-pass specimens to the average PM microhardness, a slight positive correlation between microhardness and the number of weld passes (refer Fig. 9a). Therein, the data indicates five-pass specimen displayed the maximum 8% rise in microhardness as compared to PM, owing to the most uniform Si particulate distribution, porosity reduction along with FSP led grain refinement. This suggests making multi-pass FSP, under parameters: 1500 rotation min^{-1} and 10 mm s^{-1}, add only trivial value with respect to increasing microhardness.
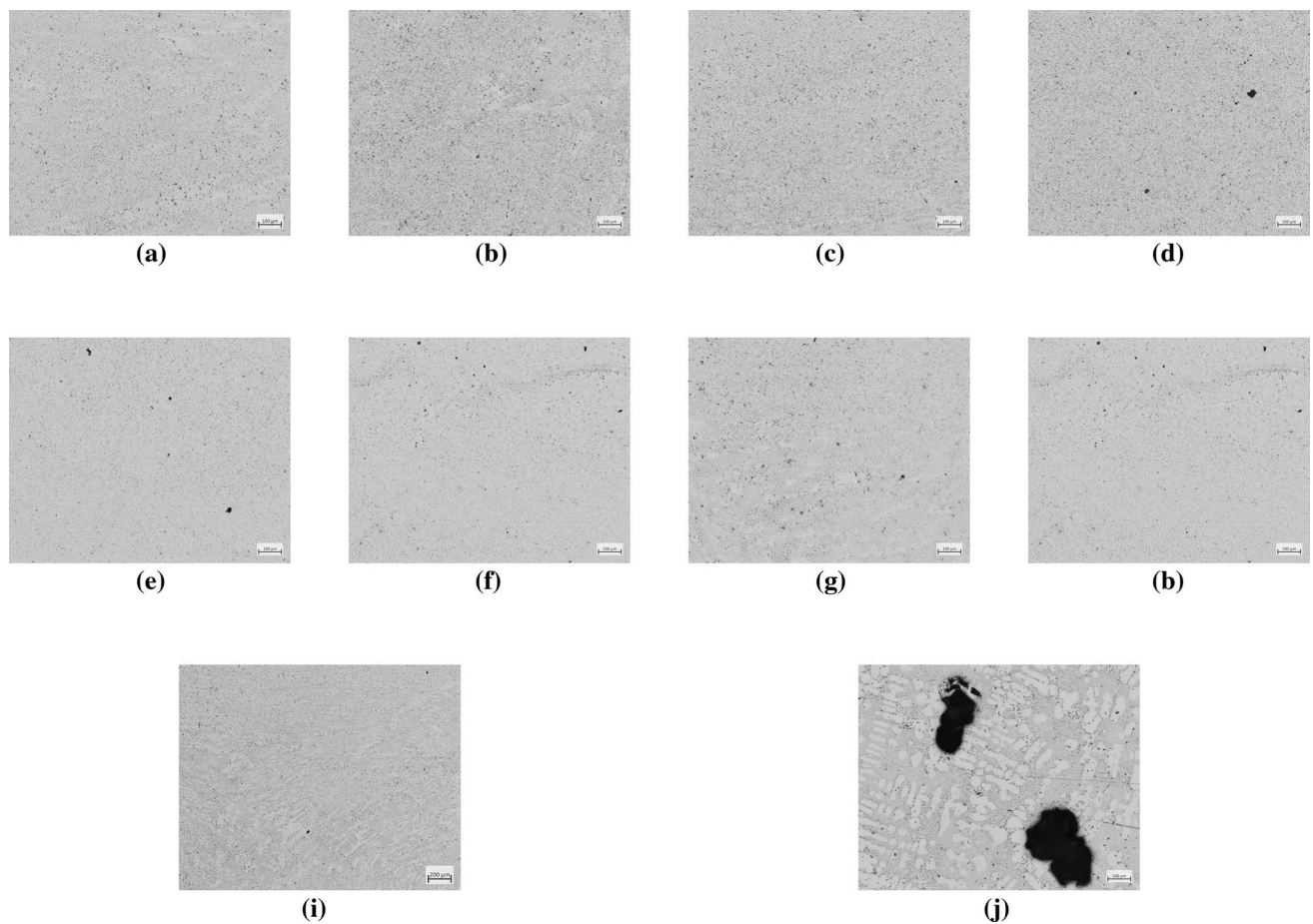
Fig. 7 Porosity map for various non FSPed and FSPed specimens: **a** R2000101×10 **b** R1500101×10 **c** R1500102×10 **d** R1500103×10 **e** R1500104×10 **f** R1500105×10 **g** R0800101×10 **h** R0800051×10 **i** R1000101×10 **j** PM×10
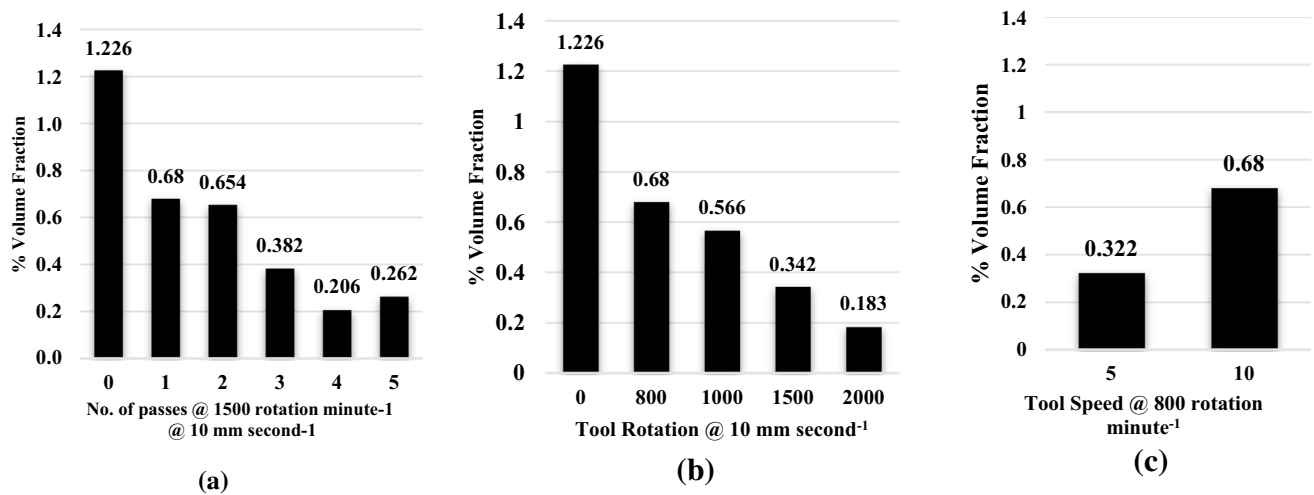
Fig. 8 Porosity measurements for FSP samples produced at different process parameters: **a** number of passes, **b** tool rotational speed, **c** travel speed

Table 3 Material displacement depth versus number of passes for experiments carried out at 1500 rotation min^{-1}

Number of passes	Depth (μm)
1	210
2	217
3	307
4	371
5	424

Identical outcomes have also been reported by Premnath et al. for Al–SiC alloy fabricated through FSP [57]. This is due to the FSP attribute of refining the microstructure which implies that for the first-pass only the Si particle refinement is accompanied by the grain refinement of α aluminium whereas during further passes the grains were not considerably refined and also for a few instances they had grown; highly dependable on the thermal cycle as discussed in Sect. 3.2. This phenomenon is quite backed by the findings of Rao et al. for FSP of cast Al–30Si alloy, in which the grains were refined upon the first pass with no substantial variation up to a further 6 FSP passes. Identical results were reported by Moslem et al. where inverse relation between average grain size and NP up to 8 has been reported [53]. In unison, if the uniformity perspective is taken into the consideration then multiple FSP passes are more appreciative industry-ready approaches as compared to an increase in TR in the course of FSP.
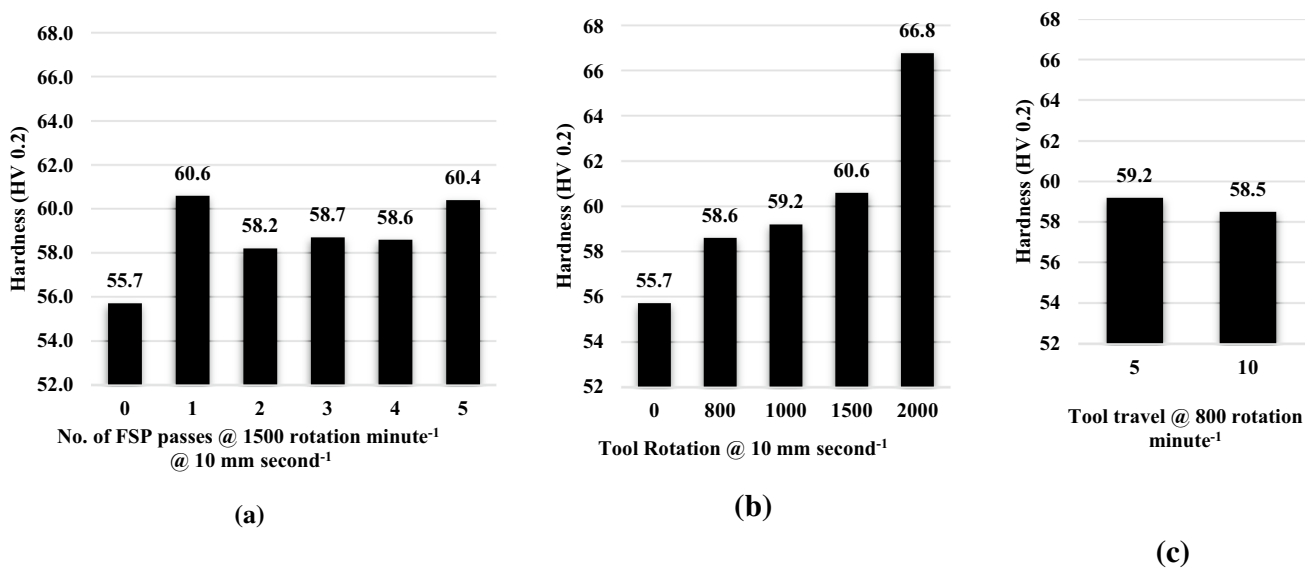
Fig. 9 Microhardness distribution for all FSP samples at different parameters: **a** number of passes, **b** tool rotational speed, **c** travel speed

Fig. 10 Microhardness standard deviation for FSP samples
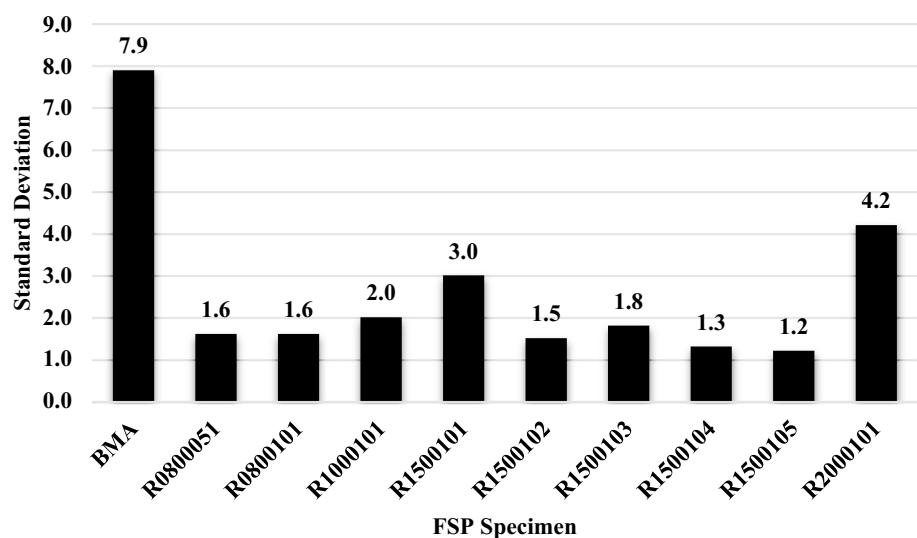
4 Conclusions

Through the present endeavour, the pivotal role of FSP attributes on the property augmentation of hypereutectic Al-Si alloy has been swotted with interesting outcomes. To this end, impacts of tool rotation speed, feed, and number of FSP passes on Si particulate and grain size alteration, the volume fraction of porosity, and microhardness were investigated. Followings are the conclusions extracted:

Almost immaculate Al-Si composite structure was realized through the set of FSP experiments. Amid all explored FSP variables tool rotation speed and number of FSP passes delivered the most favourable outcomes. Both the parameters established an almost positive correlation with defects omission and thereby mechanical properties.

The sample FSPed with uppermost tool rotation of 2000 rotation min^{-1} displayed the highest peak temperature ensuing the finest grains with high angle grain boundaries and commendable downing in the Si particulate dimensions and porosity volume fraction owing to several mechanisms like DRX and PSN. These microstructural transformations delivered the uttermost rise of 17% in microhardness by means of multiple strengthening mechanisms namely shear lag, work hardening and grain strengthening.

Multiple FSP passes have not only proven efficacy in refining the Si particles but grains too. A massive Si dendrites breakdown accompanied by even dispersion of rounded Si particulate in the nugget zone of the highest 5 pass specimen were confirmed as particulate dimensions ranging 0.5 to 5 μm and average inter-particulate spacing of 5.3 μm (96% reduction in Si lamella as compared to parent material). Simultaneously a great amount ~ 80% of porosity omission and uniform dispersion of Si particles were sources for most unwavering properties throughout the nugget of the same specimen.

Although rising the tool rotation demonstrated the peak valued properties, raising the number of passes was recognized to be a more approving approach in terms of property consistency.

5 Future Recommendations for Work and Research

Experiments in this investigation were performed with small sample sizes on a cast plate manufactured within industry standards. To further evaluate the ability to use friction stir processing as an alternative for repairing surfaced defects in aluminium–silicon castings, future research ought to be conducted on casting with a known defect, compared to repairs made using fusion welding, and future research will greatly benefit from more comprehensive measuring techniques. For instance, surface texture and porosity omission would benefit from a further investigation using alternative practices, such as processing with a stationary shoulder tool and evaluating the volume fraction of porosity using radiographic methods.

Declarations

Conflict of interests The authors have no relevant financial or non-financial interests to disclose.

Ethics Approval We confirm that manuscript has been approved by all authors for publication. I would like to declare on behalf of all co-authors that the work described herein is original research and that has not been published previously.

Consent to Participate Not applicable.

Consent for Publication Not applicable.

Research Involving Human Participants and/or Animals Not applicable.

Informed Consent Not applicable.

References

1. J.G. Kaufman, E.L. Rooy, *Aluminum Alloy Castings: Properties, Processes, and Applications* (ASM International, Materials Park, 2004)
2. R. Monroe, AFS Trans. **113**, 519 (2005)
3. P.N. Rao, *Manufacturing Technology* (McGraw-Hill Education (India), New Delhi, 2013)
4. S. Viswanathan, D. Apelian, R.J. Donahue, B. DasGupta, M. Gywn, J.L. Jorstad, R.W. Monroe, M. Sahoo, T.E. Prucha, D. Twarog (ed.), *ASM Handbook Volume 15: Casting* (ASM International, Materials Park, 2008)
5. H. Ye, J. Mater. Eng. Perform. **12**, 288 (2003)
6. K. Basavakumar, P. Mukunda, M. Chakraborty, Mater. Charact. **59**, 283 (2008)
7. S. Rathee, S. Maheshwari, A.N. Siddiquee, Mater. Manuf. Process. **33**, 239 (2018)
8. O. Elsebaie, A.M. Samuel, F.H. Samuel, H.W. Doty, Mater. Design **60**, 496 (2014)
9. K.A. Abuhasel, M.F. Ibrahim, E.M. Elgallad, F.H. Samuel, Mater. Design **91**, 388 (2016)
10. R. Counselman, Repair welding of castings, in *ASM Handbook, Vol. 15: Casting*, ed by S. Viswanathan, D. Apelian, R.J. Donahue, B. DasGupta, M. Gywn, J.L. Jorstad, R.W. Monroe, M. Sahoo, T.E. Prucha, D. Twarog, (ASM International, Materials Park, 2008)
11. J. Weritz, Aluminum alloy nomenclature and temper designations, in *ASM Handbook, Vol. 2A: Aluminum Science and Technology*, ed by K. Anderson, J. Weritz, J.G. Kaufman (ASM International, Materials Park, 2018), pp. 3–30
12. G. Gegel, D. Hoefert, J. Hirvela, R. Oehrlein, Int. J. Metalcast. **7**, 43 (2013)
13. M. Shamanian, H. Mostaan, M. Safari, M.S. Dezfooli, Metall. Res. Technol. **114**, 213 (2017)
14. J. Jiang, J. Shi, Y. Yao, A. Ma, D. Song, D. Yang, J. Chen, F. Lu, J. Mater. Eng. Perform. **24**, 2016 (2015)
15. A. Ma, K. Suzuki, N. Saito, Y. Nishida, M. Takagi, I. Shigematsu, H. Iwata, Mater. Sci. Eng. A **399**, 181 (2005)
16. S.M. Aktarer, D.M. Sekban, O. Saray, T. Kucukomeroglu, Z.Y. Ma, G. Purcek, Mater. Sci. Eng. A **636**, 311 (2015)
17. R.S. Mishra, Z. Ma, I. Charit, Mater. Sci. Eng. A **341**, 307 (2003)
18. K. Colligan, Weld. J. **78**, 229–s (1999)
19. N. Saini, C. Pandey, S. Thapliyal, D.K. Dwivedi, Silicon **10**, 1979 (2018)
20. S. Sudhagar, P.M. Gopal, Silicon **14**, 4207 (2022)
21. N. Sun, D. Apelian, Int. J. Metalcast. **13**, 234 (2019)
22. A.G. Rao, V.P. Deshmukh, N. Prabhu, B.P. Kashyap, Mater. Lett. **159**, 417 (2015)
23. S. Meenia, F. Khan, S. Babu, R.J. Immanuel, S.K. Panigrahi, G.D.J. Ram, Mater. Charact. **113**, 134 (2016)
24. V.K. Parikh, V.J. Badheka, A.D. Badgujar, N.D. Ghetiya, Mater. Manuf. Process. **36**, 1604 (2021)
25. A.G. Rao, V.A. Katkar, G. Gunasekaran, V.P. Deshmukh, N. Prabhu, B.P. Kashyap, Corros. Sci. **83**, 198 (2014)
26. T.S. Mahmoud, Surf. Coat. Tech. **228**, 209 (2013)
27. S. Joshi, R.C. Singh, R. Chaudhary, Mater. Res. Express **6**, 056554 (2019)
28. Y. Yang, P. Hua, X. Li, K. Chen, W. Zhou, Phys. Met. Metall. **120**, 1126 (2019)
29. R. Prasad, S.P. Tewari, J.K. Singh, Mater. Res. Express **6**, 096579 (2019)
30. Z. Lv, S. Han, W. Hu, Z. Dong, R. Huang, K. Yang, J. Mater. Eng. Perform. **29**, 5886 (2020)
31. A. Silva-Magalhães, J. De Backer, J. Martin, G. Bolmsjö, J. Manuf. Process. **39**, 12 (2019)
32. H. Rana, V. Badheka, Proc. Inst. Mech. Eng. L J. Mat. **233**, 977 (2019)
33. H. Rana, V. Badheka, J. Mater. Process. Tech. **255**, 795 (2018)
34. Ø. Frigaard, Ø. Grong, O.T. Midling, Metall. Mater. Trans. A **32**, 1189 (2001)
35. P. Patel, H. Rana, V. Badheka, V. Patel, W. Li, Weld. World **64**, 365 (2020)
36. K, Colligan, Friction stir welding of aluminum alloys, in *ASM Handbook, Vol. 2A: Aluminum Science and Technology*, ed by K. Anderson, J. Weritz, J.G. Kaufman (ASM International, Materials Park, 2018), pp. 748–762
37. Z. Chen, H. Ding, R. Chen, J. Guo, H. Fu, Sci. Rep. **9**, 5518 (2019)
38. J. Fan, J. Liu, S. Tian, S. Wu, S. Wang, H. Gao, J. Guo, X. Wang, Y. Su, H. Fu, J. Alloy. Compd. **650**, 8 (2015)
39. N. Hansen, Scripta Mater. **51**, 801 (2004)
40. A.V. Sergueeva, V.V. Stolyarov, R.Z. Valiev, A.K. Mukherjee, Scripta Mater. **45**, 747 (2001)
41. M. Warmuzek, in *Aluminum-Silicon Casting Alloys: Atlas of Microfractographs* (ASM International, Materials Park, 2004), pp. 1–10
42. M. Warmuzek, in A*luminum-Silicon Casting Alloys: Atlas of Microfractographs* (ASM International, Materials Park, 2004), pp. 107–114
43. K. Gao, S. Basak, M. Mondal, S. Zhang, S.-T. Hong, S.Y. Boakye, H.-H. Cho, J. Mater. Res. Technol. **17**, 3221 (2022)
44. S. Basak, M. Mondal, K. Gao, S.-T. Hong, S.Y. Anaman, H.-H. Cho, Mater. Sci. Eng. A **832**, 142490 (2022)
45. U. Chakkingal, A.B. Suriadi, P.F. Thomson, Mater. Sci. Eng. A **266**, 241 (1999)
46. F.J. Humphreys, M. Hatherly, *Recrystallization and Related Annealing Phenomena*, 1st edn. (Pergamon, Oxford, 1995)
47. A. Moharrami, A. Razaghian, M. Paidar, M. Šlapáková, O.O. Ojo, R. Taghiabadi, Mater. Chem. Phys. **250**, 123066 (2020)
48. R. Taghiabadi, A. Rostamabadi, S. Tasvibi, M.H. Shaeri, Mater. Chem. Phys. **243**, 122627 (2020)
49. V.V. Patel, V. Badheka, A. Kumar, J. Mater. Process. Tech. **240**, 68 (2017)
50. R.A. Behnagh, M.K.B. Givi, M. Akbari, Mater. Manuf. Process. **27**, 636 (2012)
51. H. Eftekharinia, A.A. Amadeh, A. Khodabandeh, M. Paidar, Rare Metals **39**, 429 (2020)
52. D. Yadav, R. Bauri,Mater. Sci. Forum **753**, 50 (2013)
53. M. Paidar, O.O. Ojo, H.R. Ezatpour, A. Heidarzadeh, Surf. Coat. Tech. **361**, 159 (2019)
54. R.S. Mishra, Z. Ma, Mater. Sci. Eng. R Rep. **50**, 1 (2005)
55. H. Rana, V. Badheka, A. Kumar, A. Satyaprasad, Mater. Manuf. Process. **33**, 534 (2018)
56. H.G. Rana, V.J. Badhek, A. Kumar, Fabrication of Al7075/B4C surface composite by friction stir processing (FSP) and investigation on hardness. Paper presented at the International Conference on Friction Based Processes-2014, Indian Institute of Science, Bengaluru, 3–5 September 2014
57. A. Premnath, Silicon **12**, 665 (2020)
58. F.J. Humphreys, M.G. Ardakani, Acta Metall. Mater. **42**, 749 (1994)
59. Q. Liu, L. Ke, F. Liu, C. Huang, L. Xing, Mater. Design **45**, 343 (2013)
60. R. George, K.T. Kashyap, R. Rahul, S. Yamdagni, Scripta Mater. **53**, 1159 (2005)
61. M. Paidar, D. Bokov, S. Mehrez, O.O. Ojo, V.V. Ramalingam, S. Memon, Surf. Coat. Tech. **426**, 127797 (2021)